

# Structural and electrochemical properties of scales formed on steel surface in CO<sub>2</sub>-rich brine at high pressure

Natália Feijó Lopes<sup>a,\*</sup>, Maryna Taryba<sup>b</sup>, João Carlos Salvador Fernandes<sup>b,c</sup>, Eleani Maria da Costa<sup>a</sup>

<sup>a</sup> School of Technology, Pontifical Catholic University of Rio Grande do Sul, 6681 Ipiranga Avenue, Building 30, Room 111/F, 90619-900 Porto Alegre, RS, Brazil

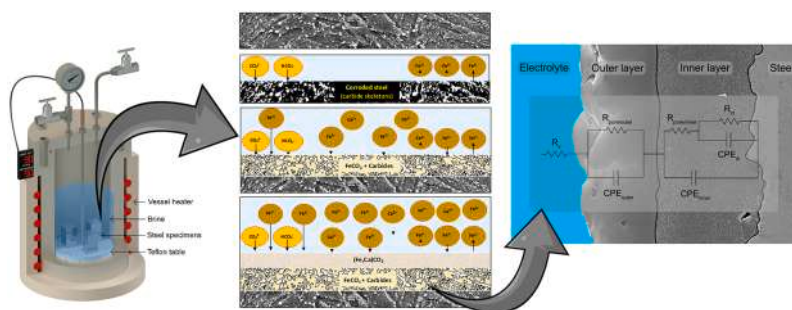
<sup>b</sup> CQE - Centro de Química Estrutural, Av. Rovisco Pais 1, 1049-001 Lisboa, Portugal

<sup>c</sup> Instituto Superior Técnico, Chemical Engineering Department, University of Lisbon, Av. Rovisco Pais 1, 1049-001 Lisboa, Portugal

## HIGHLIGHTS

- The corrosion of API L80 steel was investigated in CO<sub>2</sub>-rich brine at HPHT.
- The corrosion scale properties formed in different environments are discussed.
- General corrosion rates are highest at lower temperature.
- FeCO<sub>3</sub> scales are composed for two layers which provide different steel protection.
- Corrosion scales can act as a barrier to the diffusion of ionic species.

## GRAPHICAL ABSTRACT



## ARTICLE INFO

### Keywords:

Steel corrosion  
CO<sub>2</sub> corrosion  
High pressure  
Scale properties

## ABSTRACT

The corrosion of API L80 steel used for oil wellbore is investigated in CO<sub>2</sub>-rich brine at high pressure and temperature. The effect of protective corrosion scales associated with different variables in CO<sub>2</sub> environments is also discussed. Analyses of corrosion products formed on steel surface is conducted using FE-SEM/EDS, Raman spectroscopy and XRD. Potentiodynamic polarization and EIS are performed on corroded specimens and electrical equivalent circuit is proposed to describe the behavior of scales. Mass loss tests conducted on specimens corroded at 50 °C and 90 °C in brine saturated with CO<sub>2</sub> at 15 MPa showed that corrosion rates are higher at lower temperatures. The scales formed on the steel surface are predominantly composed of FeCO<sub>3</sub> enriched with calcium. The electrochemical protective performance of the scales is enhanced with increasing temperature. It was concluded that a long-term satisfactory performance of the scale also depends on the time and temperature of exposure to CO<sub>2</sub> environment.

## 1. Introduction

Steel corrosion is still an issue of concern for the oil industry,

especially in aqueous environments with dissolved gases such as CO<sub>2</sub>, H<sub>2</sub>S and O<sub>2</sub> [1–3]. CO<sub>2</sub> may originate from the natural composition of the reserve and/or from CO<sub>2</sub> injections, used for Enhanced Oil Recovery

\* Corresponding author.

E-mail address: [nataliaflopes@gmail.com](mailto:nataliaflopes@gmail.com) (N.F. Lopes).

<https://doi.org/10.1016/j.supflu.2022.105834>

Received 17 August 2022; Received in revised form 21 December 2022; Accepted 24 December 2022

Available online 27 December 2022

0896-8446/© 2022 Elsevier B.V. All rights reserved.

**Table 1**  
Chemical composition of the L80 API steel for casing and tubing.

Elements (wt%)													
C	Si	Mn	P	S	Cr	Mo	Ni	Al	Co	Cu	Ti	Fe	
0.257	0.18	1.07	0.006	0.002	0.31	0.05	0.01	0.048	0.005	0.005	0.046	balance	

(EOR) and Carbon Capture and Storage (CCS) purposes [4–6]. The water depth of offshore oil production increased with advanced technology, going from shallow to ultra-deep water. One example of ultra-deep water exploration is the discovery of huge volumes of light oil (28–30 degrees API) in the pre-salt reservoirs in Santos Basin, Brazil. Compared to other oil fields, the corrosion control in the pre-salt is more critical because the oil is extracted with brine and high CO<sub>2</sub> content (more than 60% CO<sub>2</sub> in some fields) at high pressure [7,8]. Therefore, these reservoir conditions have significant potential to induce high levels of corrosivity. Considering that operating conditions have grown in complexity, it is fundamental to understand the corrosive process in order to selecting steels and developing new materials for application in the oil industry [9]. Besides, there is great interest in obtaining corrosion data in conditions that cause high severity of corrosion, expected in the pre-salt environment.

It is known that approximately 60% of failures in oil fields installations are related to CO<sub>2</sub> corrosion, mainly due to incorrect corrosion prediction and low corrosion resistance of commonly used steels, such as carbon steel and high strength low alloy steel (HSLA) [10,11]. CO<sub>2</sub> corrosion is a complex process, whose mechanisms need to be better understood due to the many interdependent variables involved [11,12]. Although more than 70% of current oil and gas fields around the world are being explored at high depths and consequently high pressures [3, 13–15], there are relatively few publications addressing CO<sub>2</sub> steel corrosion in environments with these conditions. Depending on environmental factors and variables such as temperature, CO<sub>2</sub> partial pressure, pH and exposure time, among others, the steel may suffer from corrosion at low rate due to the formation of a protective layer of iron carbonate (FeCO<sub>3</sub>) on its surface [16–19]. Furthermore, it has widely reported that the chemical composition and microstructural arrays, e.g. grain sizes, dendritic spacings, among others factors, obtained by using distinct manufacturing routes have an important role on the resulting material properties [20,21]. The steel CO<sub>2</sub>-corrosion behavior is also significantly affected by the microstructural parameters and by the resulting corrosion products layer [11,22–24]. The process of growth of the FeCO<sub>3</sub> layer is typically described using the following reactions:



Thus, the global reaction of CO<sub>2</sub> corrosion can be described by Eq. 7:



As mentioned above, iron carbonate (FeCO<sub>3</sub>) plays a crucial role in defining the CO<sub>2</sub> corrosion rate of steel. Research in the CO<sub>2</sub> corrosion field has been focusing mainly on the study of stability, microstructure and composition of scale formed by corrosion products [15,25,26]. The electrochemical properties of these corrosion products also influence steel protection, once the scale may act as a diffusion barrier to electrochemically active species involved in cathodic reactions [14,27,28]. However, most studies that use electrochemical techniques to investigate the formation of iron carbonate during the corrosion process are

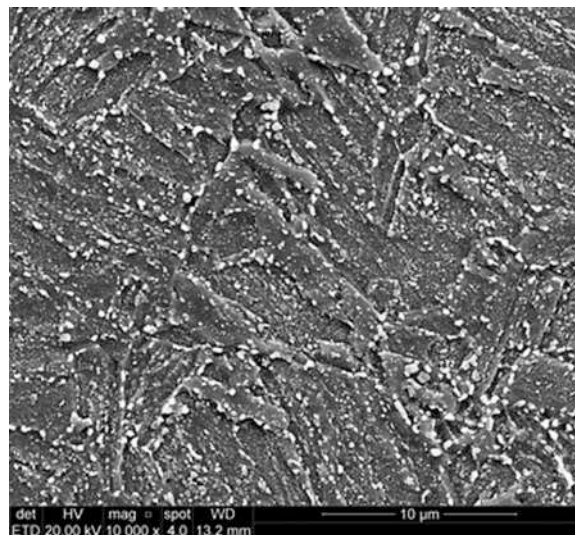


**Fig. 1.** Microstructure of the API 5CT steel constituted by acicular ferrite, bainite and globular carbides. 3% (v/v) Nital etch.

conducted at atmospheric pressure or at low CO<sub>2</sub> pressures [29,30]. There are limited studies that use electrochemical techniques to investigate anti-corrosion properties of the scales previously formed on the steel surface in CO<sub>2</sub> rich environments at high pressure and high temperature (above CO<sub>2</sub> critical point, which is at 7.38 MPa and 31.1 °C) and for long exposure periods [31]. Wu et al. [32] used the electrochemical impedance spectroscopy (EIS) technique to obtain information about the behavior of CO<sub>2</sub> corrosion using carbon steel specimens pre-corroded in water saturated with supercritical CO<sub>2</sub>, but under environmental conditions different from those of the present work. The results showed that the scale protective properties were enhanced with the increase of the exposure time (4–144 h) and temperature [28]. In this context, the objective of this study is to evaluate the performance of an API 5CT steel, grade L80, used for casing or tubing in a CO<sub>2</sub>-rich environment, with a focus on determining the properties of corrosion product scales. Brine of similar chemical composition to the water of pre-salt formations was used and the corrosion tests were performed at high pressure (15 MPa) and for long exposure periods (7 and 30 days). After the corrosion induction, analyses of microstructure and composition of corrosion products scales were correlated to the results of electrochemical properties in aerated Na<sub>2</sub>SO<sub>4</sub> solution to better reveal the anti-corrosion properties of scales formed on the steel surface.

## 2. Experimental procedures

### 2.1. Materials

The steel specimens used in this study were obtained from a section of a L80 API 5CT steel used for casing or tubing. The chemical composition of the steel, obtained by optical emission spectrometry (OES), is shown in Table 1. The values in Table 1 correspond to average of three measurements. The steel chemical composition is according with the specification of API 5CT [33]. The microstructure is constituted by acicular ferrite, bainite and globular carbides (Fe<sub>3</sub>C) precipitated at grain boundaries (Fig. 1).

**Table 2**  
Chemical composition of the brine.

Salt (Reagent grade)	Concentration (mg.L <sup>-1</sup> )
NaCl	11,400
KCl	442
CaCl <sub>2</sub> ·2 H <sub>2</sub> O	74
MgCl <sub>2</sub> ·6 H <sub>2</sub> O	72

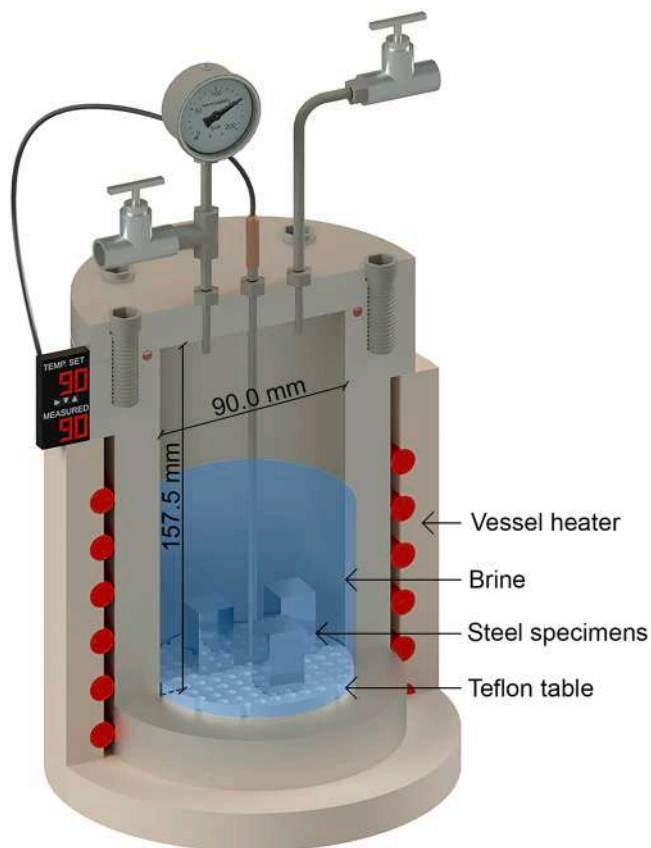


**Fig. 2.** Schematic arrangement of corrosion tests in Parr autoclave.

Prior to the corrosion tests, the prismatic specimens with dimensions of approximately 9×9×6mm were ground with SiC papers in the sequence # 220, # 320, #400, #600 and #1200, cleaned with acetone in an ultrasound bath for 5 min and subsequently weighed using a 0.0001 g precision balance.

The composition of the brine, used in corrosion tests, is presented in Table 2. The reagents were weighed in a 0.0001 g precision balance. This composition is similar to the brine of pre-salt formations in Santos Basin, Brazil. The brine pH is 6.09 at NTP (normal temperature and pressure). However, the corrosion tests were designed to reproduce pHs equivalent to those found in pre-salt formations in Santos Basin. The pHs of brine saturated with CO<sub>2</sub> at 15 MPa calculated by thermodynamic model [34] are 3.05 and 3.15 at 50 °C and 90 °C, respectively.

## 2.2. Autoclave CO<sub>2</sub> corrosion tests to prepare corrosion product scales

The CO<sub>2</sub> corrosion tests to form corrosion product scales were conducted in a 1 L pressure vessel made of titanium alloy (Ti-6Al-4 V). Three prismatic specimens of approximately 9×9×6mm were placed on a Teflon® table (with openings to allow the contact of specimens with solution) into the vessel, as illustrated in Fig. 2. For each individual test, the brine volume was 300 mL. Before pressurizing the system, the brine

was deaerated by N<sub>2</sub> bubbling for one hour, followed by CO<sub>2</sub> bubbling for another hour. The corrosion tests were performed at temperatures of 50 ± 0.5 °C and 90 ± 0.5 °C, for periods of 7 and 30 days. The vessel was heated to desired temperature, and the system was pressurized with CO<sub>2</sub> 99.9% purity (Air Products) to achieve 15 ± 1.0 MPa. This experimental arrangement creates two phases into the vessel, CO<sub>2</sub> saturated brine at lower part of the vessel and wet supercritical CO<sub>2</sub> at upper part of the vessel. The specimens were immersed in CO<sub>2</sub> saturated brine phase. The CO<sub>2</sub>-rich phase at the top of the vessel supplies the CO<sub>2</sub> consumption during the corrosion process ensuring that the pH remains stable during the corrosion tests. The corrosion tests were performed in static conditions (no flow or brine stirring).

After the corrosion test period, the vessel was depressurized and the steel specimens were washed with Milli-Q water, acetone, dried with hot air and maintained in desiccator for further analysis.

## 2.3. Determination of CO<sub>2</sub> corrosion rates

Mass loss tests were conducted according to ASTM G1-03 (standard practice for preparing, cleaning, and evaluating corrosion on test specimens) [35] to obtain general corrosion rates. The scale formed under CO<sub>2</sub> environments was removed from the surface of specimens by immersion in acid solution (HCl and distilled water at 1:1 proportion with addition of 3.5 g.L<sup>-1</sup> hexamethylenetetramine) at room temperature. Each specimen was submerged in the solution for 30 s, washed in distilled water and acetone, dried and weighed using a 0.0001 g precision balance. This procedure was repeated for at least 20 times until constant mass loss was observed. The general corrosion rate (CR) was determined by Eq. 8.

$$CR = \frac{K \cdot \Delta w}{A \cdot t \cdot \rho} \quad (8)$$

K is a constant (for mm.y<sup>-1</sup> is 8.76 × 10<sup>4</sup>), Δw is weight loss in grams, A is the surface area of specimen in cm<sup>2</sup>, t is the time of exposure in hours, and ρ is density of steel.

## 2.4. Characterization of corrosion scales formed under CO<sub>2</sub> environment

### 2.4.1. Analyses of morphology and composition of scales

The morphology and thickness of scales grown on the steel surface were investigated by using field emission scanning electron microscopy (FE-SEM), model Inspect F50-FEI. The chemical composition of the corrosion scales on specimen surface was analyzed by EDS using FE-SEM and by X-ray diffraction (XRD) on a D8 Advance Bruker AXS θ-2θ diffractometer with a copper radiation source (Cu Kα, λ = 1.5406 Å) and a secondary monochromator, operating at 40 kV and 40 mA. Raman spectroscopy was also performed, using a Horiba LabRAM HR800 Evolution equipment using a radiation source with a solid-state laser operating at 532 nm with an output power of 20 mW, a spectrograph with a 600 lines.mm<sup>-1</sup> grating. Raman spectroscopy was used at a 10x magnitude lens with 50% filter and wavelength range of 100–1800 cm<sup>-1</sup>.

### 2.4.2. Electrochemical analyses

Potentiodynamic polarization (PP) and electrochemical impedance spectroscopy (EIS) were conducted to obtain information about the electrochemical properties of the corrosion scale in terms of steel protection. The measurements were carried out by Autolab PGSTAT 302 N potentiostat, at atmospheric pressure and room temperature, using a classical three-electrode configuration: a working electrode (steel covered with scale), saturated calomel reference electrode and a platinum auxiliary electrode. It is important to mention that is difficult to carry out electrochemical measurement in autoclave once it requires special electrodes that can withstand high pressure (15 MPa).

Electrochemical measurements were performed using the CO<sub>2</sub> pre-corroded specimens embedded in epoxy resin to allow an exposed

area of 0.5 cm<sup>2</sup>. The electrical contact was done using a copper wire and silver bond. A 0.1 M Na<sub>2</sub>SO<sub>4</sub> solution, pH= 6, was used as electrolyte. This solution was chosen because it is a strong ionic electrolyte and offers low corrosivity level to steel with low tendency to promote localized attack allowing better evaluation of the scale properties as barrier for ion migration towards steel substrate. The main chemical reaction involves the iron dissolution to forms iron sulfate [36]. Although the Na<sub>2</sub>SO<sub>4</sub> electrolyte is less corrosive, the FeCO<sub>3</sub> formed in the autoclave test could dissolve during the electrochemical measurements because the saturation degree of FeCO<sub>3</sub> would be less than 1 (low temperature, presence of O<sub>2</sub>, and absence of CO<sub>2</sub>). Furthermore, the potentiodynamic test was carried out in the potential range of - 1 and 1 V in relation to open circuit potential (OCP), which also could disturb the stability of FeCO<sub>3</sub> during the potential scan. The electrochemical tests were carried out under aerated conditions using a scan rate of 1 mV.s<sup>-1</sup>. It is remarked that potential scan rate has an important role in order to minimize the effects of distortion in Tafel slopes and corrosion current density analyses, as previously reported [37–39]. However, based on these reports, the adopted 1 mV/s has no deleterious effects on those Tafel extrapolations to determine the corrosion current densities of the examined samples. All values of potential (E) are referred in relation to the saturated calomel electrode (SCE) potential.

EIS spectra were obtained, in relation to OCP, after 1 h, 24 h and 168 h of immersion in 0.1 M Na<sub>2</sub>SO<sub>4</sub> with a sinusoidal potential excitation of 10 mV rms amplitude, in the frequency range from 100 kHz to 10 mHz, using 9 points per decade. The analysis of the impedance data involved the fitting to an equivalent circuit model that best represents the physical phenomena involved in the performance of scales as an anti-corrosion coating protector. The fitting of the impedance data to the electrical equivalent circuits was done using Zview® software.

The corrosion rates of steels in CO<sub>2</sub> environments depend on the formation of FeCO<sub>3</sub> corrosion product scales and their protective characteristics. Thus, the durability of the scales is an important property to predict the evolution of corrosion over time and it can be obtained from EIS results. To examine the different characteristics of FeCO<sub>3</sub> corrosion product scales formed at different temperatures and immersion times, the coefficients of degradation over time of the corrosion product scales in Na<sub>2</sub>SO<sub>4</sub> solution were calculated with Eq. 9 [40].

$$D_t = -\log\left(\frac{|Z|_t}{|Z|_0}\right) \quad (9)$$

where D<sub>t</sub> is the degradation coefficient, |Z|<sub>t</sub> is the impedance at t time; |Z|<sub>0</sub> is the initial impedance; and f the frequency (Hz). Usually, a low frequency (equal or close to the minimum frequency) is used for D<sub>t</sub> calculation to obtain a |Z| value that represents the contributions of the various processes occurring in the specimen.

The D<sub>t</sub> determination in aerated Na<sub>2</sub>SO<sub>4</sub> solution is useful to measure the scale stability and to estimate its capability to protect the steel when exposure to CO<sub>2</sub> environment.

As Fe<sub>3</sub>C is an electronic conductor, there are possibility of galvanic coupling between the steel substrate and the layer of undissolved Fe<sub>3</sub>C [41]. The scanning vibrating electrode technique (SVET) was used to monitor the local activity of corrosion process of scale-covered steel when in presence of an artificial mechanical damage in the scale, examining possible galvanic couple formation between steel and scale. A typical aerated 0.05 M NaCl solution (pH 6.5) was used as electrolyte due to its low conductivity (5.26 mS.cm) which is required by this technique. The specimen was embedded in epoxy resin with an exposed surface area of 1 mm<sup>2</sup>, delimited using the mixture of beeswax and colophony. An artificial defect (pinhole), with an area of about 1.2 × 10<sup>4</sup> μm, was created in the corrosion scale using a needle-shaped tool to reach the steel surface. SVET measurements were performed using commercially produced equipment and corresponding software (Applicable Electronics™ and ScienceWares™, respectively). The local current density distributions were recorded every hour in a grid of 21 × 21

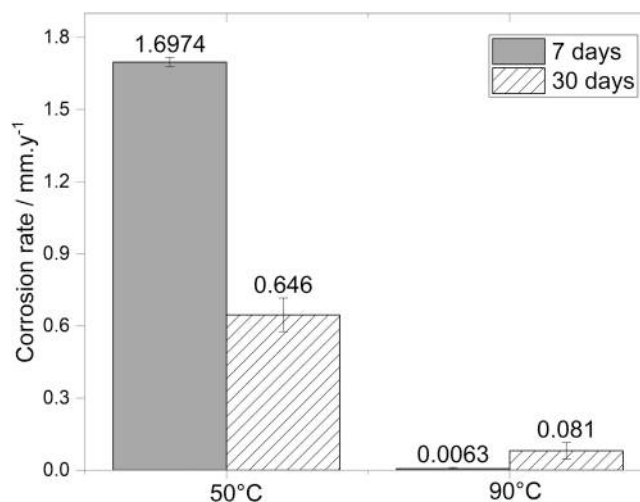


Fig. 3. General corrosion rates of steel exposed to CO<sub>2</sub> saturated brine for different temperatures and exposure times obtained by mass loss tests.

points during 24 h of immersion. An insulated Pt-Ir probe (Micro-Probes™) was used as a vibrating microprobe, after deposition of platinum black on its tip to a spherical shape of 10 μm diameter. The amplitude of vibration (pick-to-pick) was 20 μm. The probe was vibrating in both, vertical (Y) and horizontal (X) directions, but only the vertical component was considered for analysis.

### 3. Results and discussion

#### 3.1. Corrosion rates obtained by mass loss tests

Fig. 3 shows general corrosion rates calculated by mass loss for different conditions of corrosion. The corrosion rates are in the range of those reported in literature for similar environmental conditions, which usually are less than 10 mm.y<sup>-1</sup> [42,43]. CO<sub>2</sub> corrosion tests were conducted at two different temperatures (50 °C and 90 °C), presenting the highest corrosion rates in those conducted at lower temperature (≤ 1.7 mm.y<sup>-1</sup> for 50 °C and 0.08 mm.y<sup>-1</sup> for 90 °C). The solubility of CO<sub>2</sub> in water decreases as temperature increases, for temperatures up to 100 °C. Consequently, CO<sub>2</sub> solubility in brine is higher at 50 °C than at 90 °C, with solubility values at 15 MPa of 1.17 mol.kg<sup>-1</sup> and 0.97 mol.kg<sup>-1</sup>, respectively, providing a slight increasing on pH with temperature (3.05 at 50 °C and 3.15 and 90 °C) [34]. Nevertheless, the temperature accelerates all processes involved in corrosion (electrochemical, chemical, transport, among others). Therefore, in the absence of protective corrosion layers, it would be expected from this perspective that the corrosion rate would increase continuously with temperature. However, an increase in temperature may reduce the corrosion rate if it promotes the formation of a protective corrosion scale. In addition, the kinetics of FeCO<sub>3</sub> precipitation is an important factor in the protection properties of corrosion product layers. FeCO<sub>3</sub> solubility decreases, and its precipitation occurs much faster at higher temperatures [15,42,43]. Other authors have also reported a decrease in corrosion rates with an increase in temperature [32,44,45]. With exposure time of 7 and 30 days, the tests performed at 50 °C showed a decrease in the corrosion rate with time, while the tests performed at 90 °C showed an increase. These results can be related to the scale protection properties of the substrate, since the corrosion rate is higher at lower temperature and then the scale is formed earlier acting as a barrier against corrosion.

#### 3.2. Morphology and composition of corrosion scales

The morphologies of corrosion scales formed on steel surface in brine saturated with CO<sub>2</sub> and the respective EDS analyses are shown in Fig. 4.

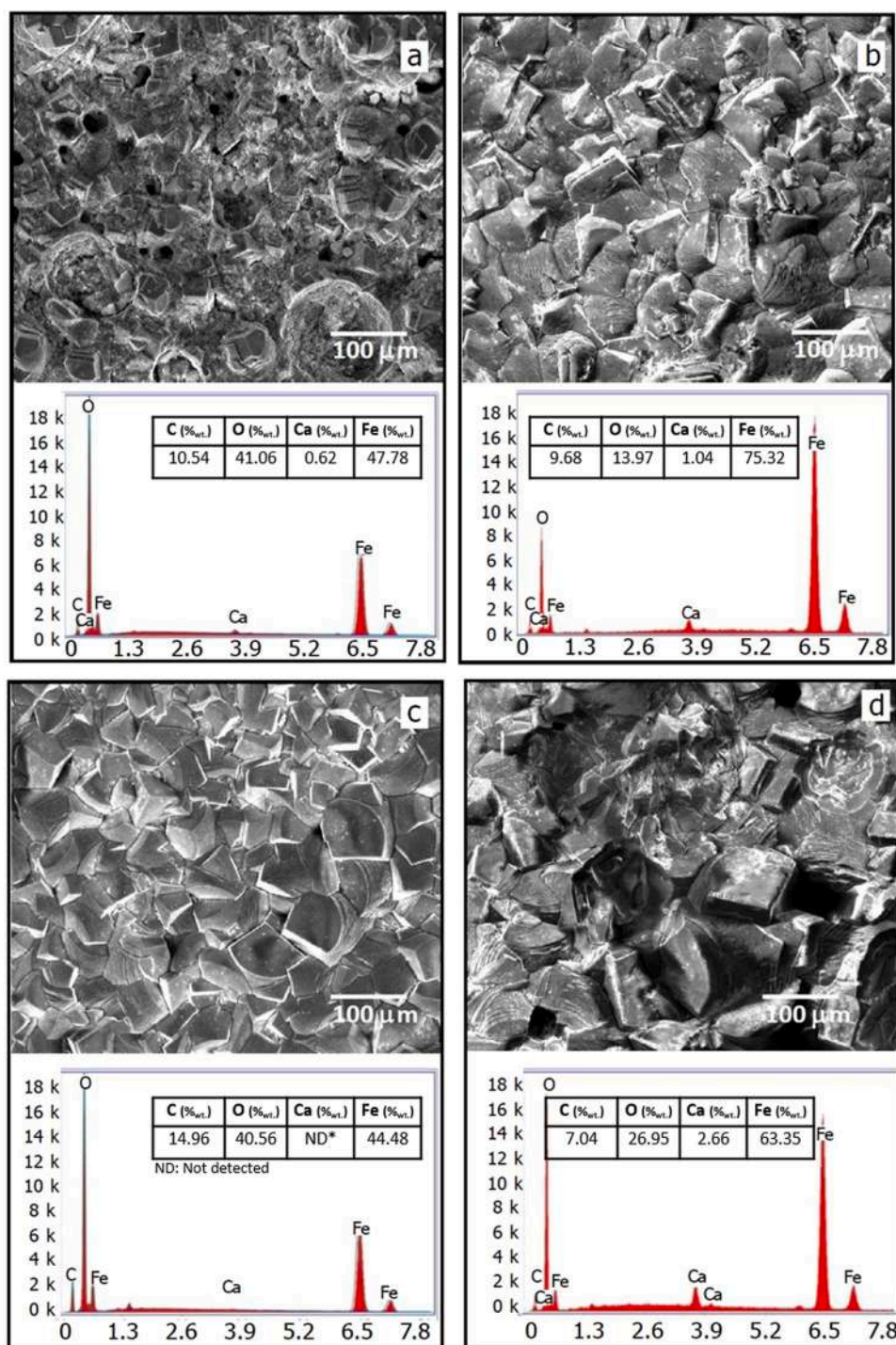


Fig. 4. Morphology and elemental composition of scales formed on steel surface due to exposure to CO<sub>2</sub> saturated brine. a) 50°C, 7 days; b) 50°C, 30 days; c) 90°C, 7 days; d) 90°C, 30 days.

The steel surface of all specimens was entirely covered by the corrosion product scale due to long time of corrosion tests. Wang et al. (2022) [42] observed that in similar condition of temperature and pressure (90 °C and 14 MPa) the scales already covered the steel surface in 24 h of exposure. The scale morphology is typical of carbonate crystals, constituted by prismatic crystals that are uniformly distributed on the surface with very few and small gaps between them. Characteristic peaks of O, C Fe and Ca elements are present in the EDS spectra of scales, indicating that most of the scales are composed of iron carbonate enriched with calcium. Table 3 shows the estimated compositions of the

scales, based on the EDS and XDR results. Ca was detected by EDS in all specimens, except for those exposed to CO<sub>2</sub> saturated brine at 90 °C for 7 days probably due to detection limit provided by this technique. As the Ca<sup>2+</sup> transport from brine to form carbonates on the steel surface is a time and temperature dependent process, it is expected to have higher Ca content in the scales formed at higher temperature and longer period. On the other side, the propensity of Ca dissolution from mixed carbonates also accelerates once the energy for loosing Ca is lower than losing Fe [38]. Ca is incorporated in iron carbonate lattice as a substitutional element. It has been reported that the incorporation of this element may

**Table 3**  
Composition of scales formed on steel surface in CO<sub>2</sub> saturated brine estimated by EDS and XRF.

Scale growth conditions	(Fe <sub>x</sub> Ca <sub>1-x</sub> CO <sub>3</sub> ) Calculated from EDS	(Fe <sub>x</sub> Ca <sub>1-x</sub> CO <sub>3</sub> ) Calculated from XRD*
50 °C, 7 days	Fe <sub>0.98</sub> Ca <sub>0.02</sub> CO <sub>3</sub>	Fe <sub>0.94</sub> Ca <sub>0.06</sub> CO <sub>3</sub>
50 °C, 30 days	Fe <sub>0.98</sub> Ca <sub>0.02</sub> CO <sub>3</sub>	Fe <sub>0.91</sub> Ca <sub>0.09</sub> CO <sub>3</sub>
90 °C, 7 days	FeCO <sub>3</sub> **	Fe <sub>0.99</sub> Ca <sub>0.01</sub> CO <sub>3</sub>
90 °C, 30 days	Fe <sub>0.94</sub> Ca <sub>0.06</sub> CO <sub>3</sub>	Fe <sub>0.99</sub> Ca <sub>0.01</sub> CO <sub>3</sub>

\* Calculated by siderite d<sub>(104)</sub> displacement

\*\* Ca non-detected

affect the steel corrosion rate [46–49].

Raman spectra combined with XRD pattern (Fig. 5) confirmed that the scales consist mainly of FeCO<sub>3</sub>. All specimens presented peaks of similar wavelengths in the Raman spectra (Fig. 5(a)), regardless of temperature and exposure time. It can be observed through the XRD pattern (Fig. 5(b)) that there is a small displacement of the diffraction

peaks to the left and an increase of the interplanar spacing in relation to standard spectra of the siderite (FeCO<sub>3</sub>), which may be associated with the presence of substitutional calcium in the lattice of FeCO<sub>3</sub>, as also indicated by EDS analysis (Table 3). This slight change on the angle of interplanar diffraction (d) is probably due to the difference in Ca and Fe atomic radius [46]. The increase of d-spacing for the plane (104) of iron-calcium carbonate for all experimental conditions is also shown in Table 3. The calculated Ca amount from XDR can be estimated more accurately than EDS, which is a semi-quantitative technique.

Fig. 6 presents the images obtained by FE-SEM of cross sections of scales. The scales are composed of two layers (inner and outer layers). The inner layer is microstructurally distinct from the outer layer. Constituted of cementite skeleton (Fe<sub>3</sub>C) and other carbides, the inner layer is probably associated with the preferential dissolution of ferrite. Cementite forms preferential low-overpotential cathodic sites and favors hydrogen evolution. This leads to formation of microgalvanic cells between carbides and ferrite, resulting in selective dissolution of ferrite and increasing the corrosion rate [51]. On the other hand, cementite may act as an additional diffusion barrier for corrosive species to reach

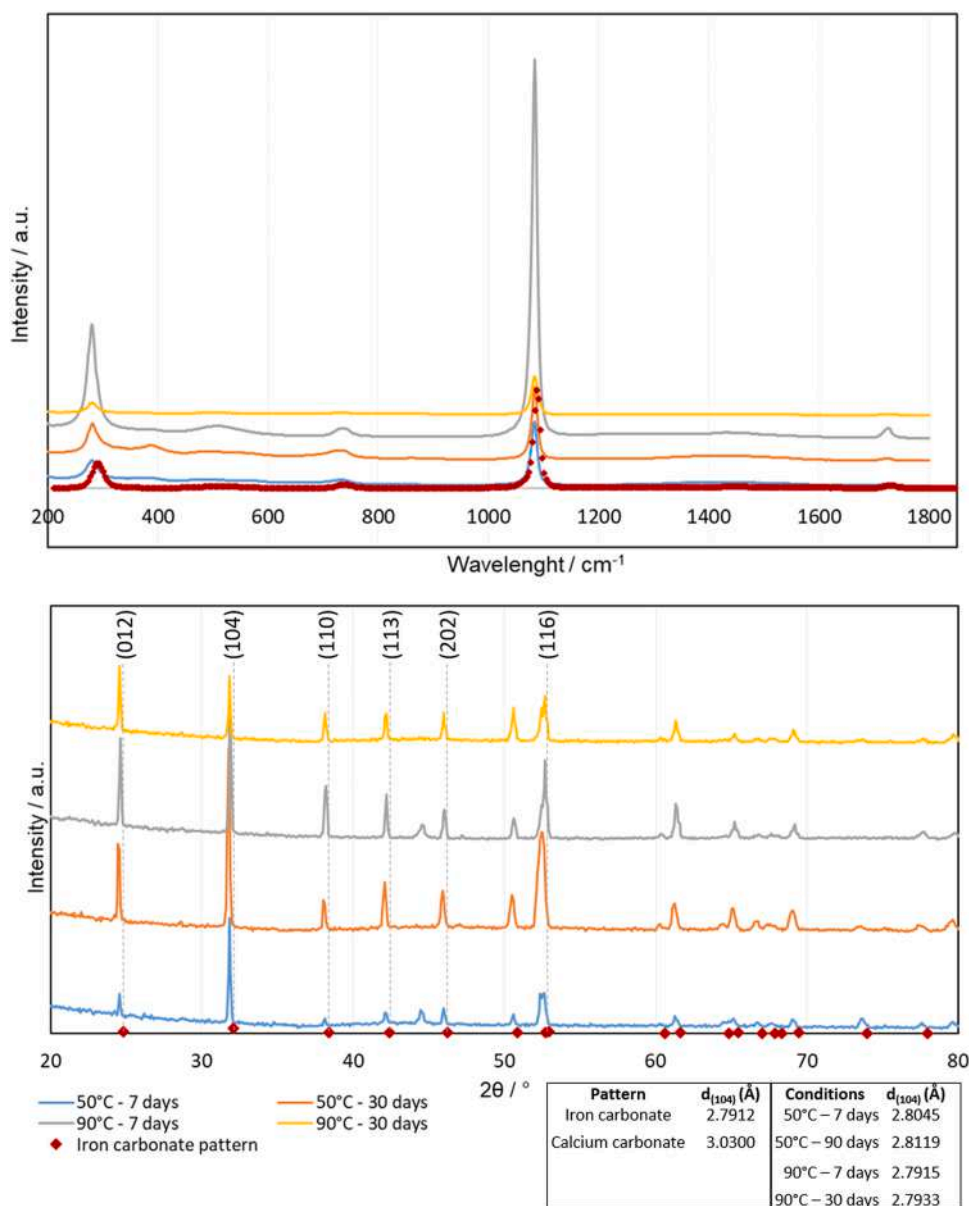


**Fig. 5.** (a) Raman spectra and (b) XRD pattern (pattern number 83–1764 from International Centre for Diffraction Data- ICDD [50]) of scale formed on steel surface in CO<sub>2</sub> saturated brine at 15 MPa for different temperatures and exposure times.

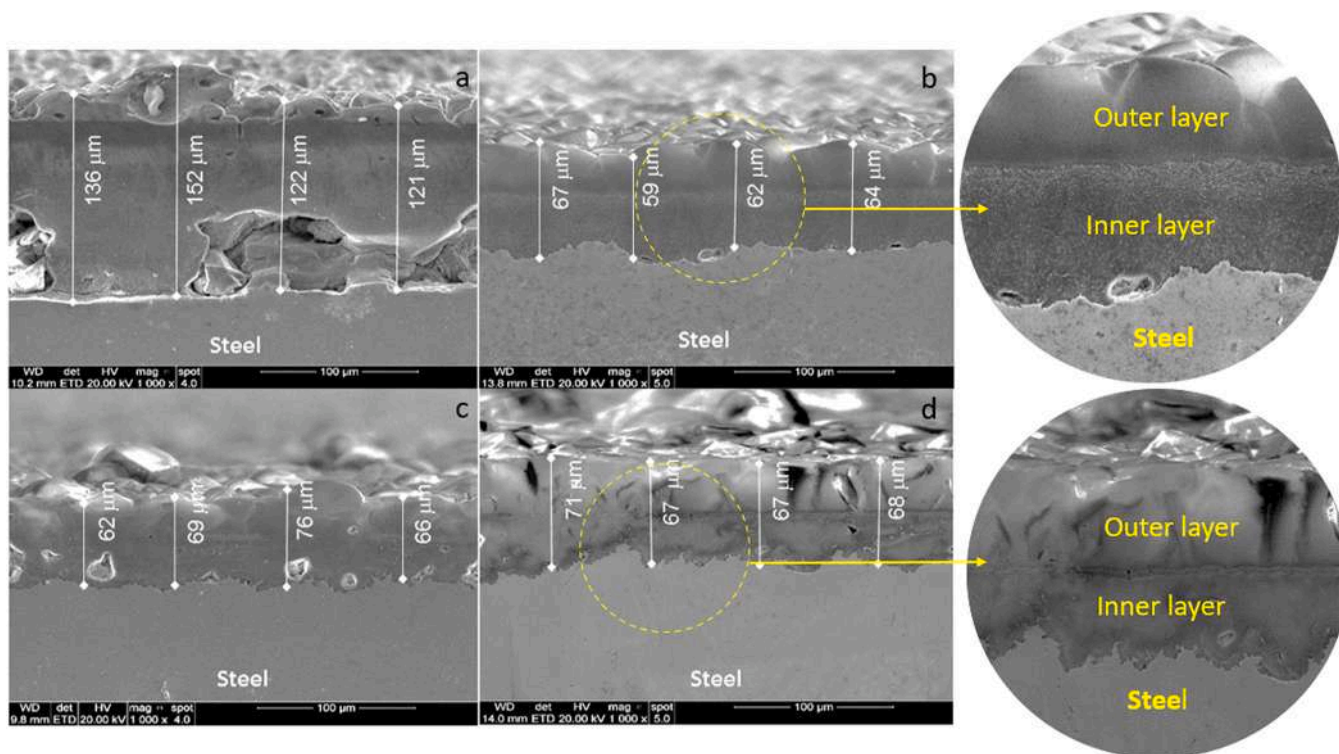


Fig. 6. FE-SEM images of cross section and EDS spectra of the scales formed on steel surface in CO<sub>2</sub> saturated brine for different temperatures and exposure periods: (a) 50 °C- 7 days. (b) 50 °C- 30 days. (c) 90 °C- 7 days. (d) 90 °C- 30 days.

Table 4

Average thickness of scales formed on the steel surface.

Scale growth conditions	Average thickness (μm)
50 °C – 7 days	151 ± 14
50 °C – 30 days	75 ± 7
90 °C – 7 days	63 ± 8
90 °C – 30 days	74 ± 8

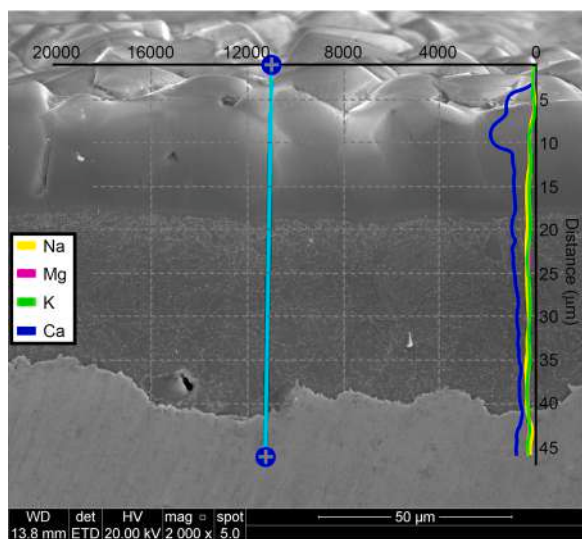


Fig. 7. EDS line scan of cross section of the scale formed on steel surface in CO<sub>2</sub> saturated brine, 50 °C for 30 days.

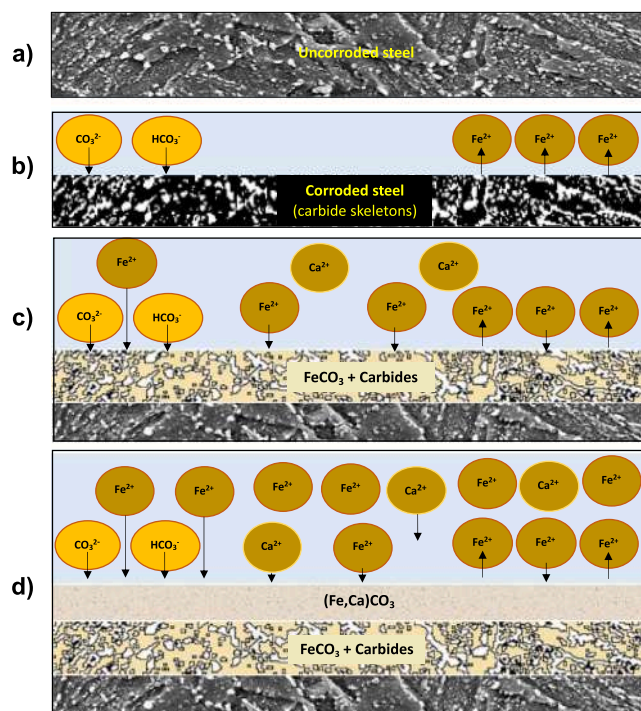
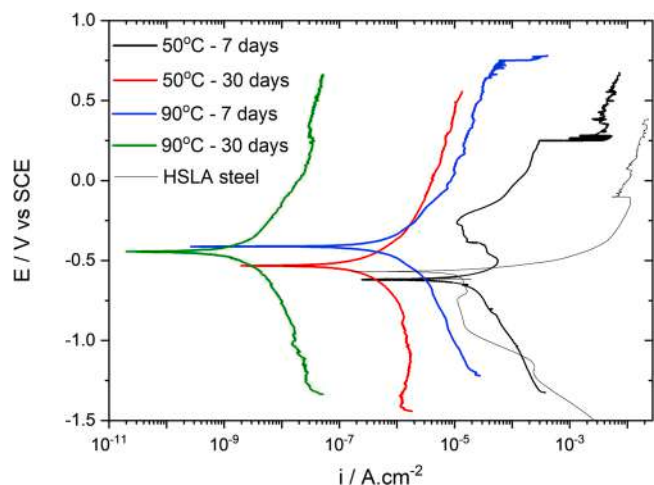


Fig. 8. Mechanism of FeCO<sub>3</sub> scale layers formation on the steel surface. (a) Un corroded steel. (b) Steel corrosion by preferential ferrite dissolution. (c) FeCO<sub>3</sub> precipitation within carbide skeletons forming the inner layer. (d) (Fe, Ca)CO<sub>3</sub> precipitation forming the outer layer.

the steel surface, leading to a slight decrease in the corrosion rate. Additionally, the FE-SEM images of Fig. 6 show that the interface between the two layers is less obvious in specimens immersed in CO<sub>2</sub>



**Fig. 9.** Polarization curves in 0.1 M Na<sub>2</sub>SO<sub>4</sub> solution for iron carbonate scales (scale-covered steel) formed in CO<sub>2</sub> saturated brine in different experimental conditions, compared with bare steel.

medium for 7 days when compared to the ones that were immersed for 30 days. The scales present some gaps between the crystals in the inner layer which is more evident in scale formed at 50 °C for 7 days (Fig. 5 (a)), indicating that it could offer poor protection to the steel. However, it is known that the protection offered by the scales depends not only on the pore size and density, but also on the pore connectivity [52]. The scales thickness (Table 4) was very similar in all growth conditions (ranging from 63 to 75 μm), with exception of the specimen exposed to 50 °C for 7 days, where the scale was two times thicker (151 μm). The

**Table 5**

Electrochemical parameters in 0.1 M Na<sub>2</sub>SO<sub>4</sub> and corrosion rate obtained from polarization curves for scales formed on the steel surface in CO<sub>2</sub> saturated brine at 15 MPa.

Scale growth conditions	$\beta_a$ (V.dec <sup>-1</sup> )	$\beta_c$ (V.dec <sup>-1</sup> )	$E_{corr}$ (mV)	$i_{corr}$ (μA.cm <sup>-2</sup> )	$R_p$ (k.cm <sup>2</sup> )	CR (mm.y <sup>-1</sup> )
HSLA steel	0.037	0.214	-574 (± 38)	310 (± 20)	1.6 (± 0.11)	3.69 (± 0.24)
50 °C, 7 days	0.820	0.299	-617 (± 1.7)	110 (± 3)	13.13 (± 0.04)	1.28 (± 0.003)
50 °C, 30 days	2.728	1.293	-533 (± 0.6)	1.94 (± 0.04)	833.71 (± 1.00)	2.2 (± 0.002) x10 <sup>-2</sup>
90 °C, 7 days	1.701	2.081	-413 (± 0.8)	1.53 (± 0.05)	259.64 (± 0.52)	6.2 (± 0.002) x10 <sup>-2</sup>
90 °C, 30 days	1.36	1.00	-442 (± 1.3)	0.086 (± 0.002)	1.72 (± 0.05) x10 <sup>5</sup>	1.0 (± 0.3) x10 <sup>-4</sup>

$\beta_a$  and  $\beta_c$  = Tafel slopes;  $E_{corr}$  = Corrosion potential;  $i_{corr}$  = Corrosion current density;  $R_p$  = Polarization resistance; CR = Corrosion rate.

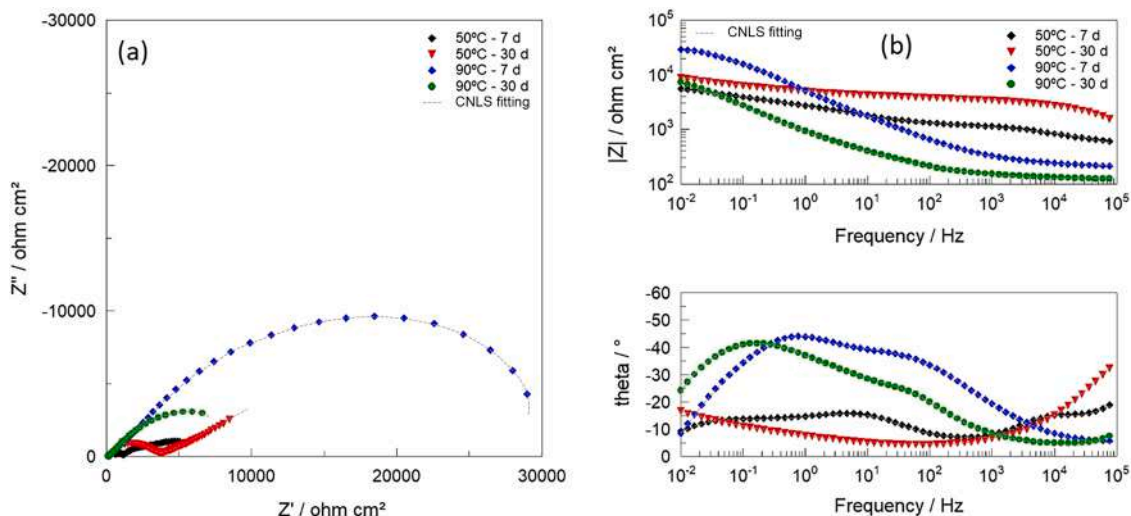


**Fig. 10.** (a) Nyquist and (b) Bode diagrams (magnitude on top and phase angle at bottom) for steel covered with scales formed in CO<sub>2</sub> saturated brine, after 168 h of immersion in 0.1 M Na<sub>2</sub>SO<sub>4</sub>.

increase in thickness exhibited for this specific scale might be explained by inner layer low compactness, since the FE-SEM images present large gaps associated with lack of filling between carbide structures with carbonates (Fig. 6(a)). The scale compactness is dependent on temperature and corrosion time. It agrees with the reported results in literature [43], showing that scales become more compact with corrosion time and with increasing on temperature and exposure time.

EDS line scan analysis (Fig. 7) of the inner and outer layers showed the different compositions of the layers. The outer layer showed an increase of Ca in the direction of the sample edge. The XRD and Raman results corroborated the FE-SEM analysis (Fig. 7), indicating that the innermost layer of the corrosion product is formed by steel corrosion and the outermost layer results from the redepositing of the FeCO<sub>3</sub> with the substitutional calcium in the crystalline lattice. The mechanism for FeCO<sub>3</sub> precipitation, forming two layers, is illustrated in Fig. 8, where the preferential dissolution of ferrite occurs and the formation of a FeCO<sub>3</sub> scale between the carbide skeletons creates the inner corrosion product layer. Then, the formation of the outer layer occurs by precipitation of iron carbonate as a result of high concentration of iron ions in the corrosive medium.

### 3.3. Electrochemical properties of corrosion scales

The polarization curves (Fig. 9) show the electrochemical performance of scales formed on CO<sub>2</sub> corroded steel surface at different environmental conditions, in comparison with uncorroded steel. Table 5 shows the respective electrochemical parameters, obtained from Tafel analysis. All scales offered steel corrosion protection in 0.1 M Na<sub>2</sub>SO<sub>4</sub>. However, the electrochemical properties of scales formed at 90 °C indicate that they are more protective to the steel surface than the ones formed at 50 °C, considering the same period of exposure to CO<sub>2</sub>

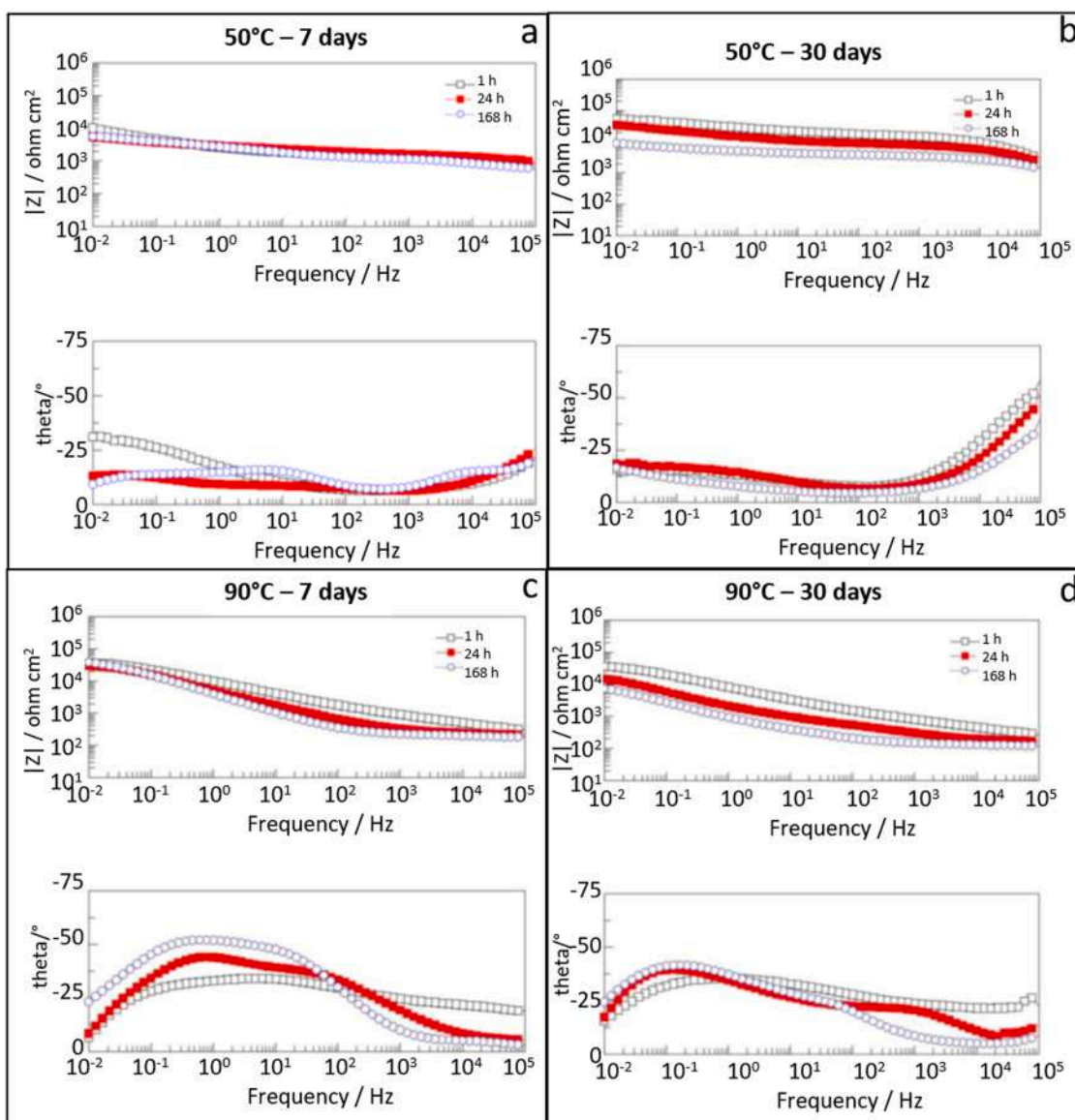


**Fig. 11.** Bode and phase angles diagrams for scales grown in CO<sub>2</sub> saturated brine for different immersion times in 0.1 M Na<sub>2</sub>SO<sub>4</sub> solution. (a) 50 °C, 7 days; (b) 50 °C, 30 days; (c) 90 °C, 7 days and (d) 90 °C, 30 days.

medium. Scales formed at 90 °C led to lower current densities ( $i_{\text{corr}}$ ), higher polarization resistance ( $R_p$ ) and less active corrosion potentials ( $E_{\text{corr}}$ ). The polarization curves show that exposure time in CO<sub>2</sub> medium influences the electrochemical scale properties and increases steel protection with time. Similar electrochemical performance of scales is expected in CO<sub>2</sub> medium at high pressure, once low  $i_{\text{corr}}$ , high  $R_p$  and less active  $E_{\text{corr}}$  are related to less porous and more compact scale, which can strengthen its protective capacity making it difficult for the corrosive agent to reach the substrate, as also observed by Wu et al., 2004 and Hua et al., 2019 [16,28]. According to polarization curve, the scale formed at 50 °C in 7 days exhibited the lowest protection properties, which can be related to the high porosity of the scale, as seen in the FE-SEM image of Fig. 5(a).

An EIS study was conducted to assess the electrochemical properties of scales and to provide more information about anti-corrosion performance since it is a non-steady technique and very surface sensitive, which makes many changes visible when compared to polarization technique. The EIS measurements were carried out for different immersion times (1 h, 24 h, and 168 h) in Na<sub>2</sub>SO<sub>4</sub> solution.

The Nyquist and Bode diagrams obtained from EIS for all steel

samples covered with distinct scales after immersion in 0.1 M Na<sub>2</sub>SO<sub>4</sub> for 168 h are shown in Fig. 10. Nyquist plot (Fig. 10(a)) of the scale formed at 50 °C/7 days show two capacitive semicircles, characterizing active corrosion at the interface when scale is exposed to the electrolyte. This behavior is typical of a material covered by a porous layer with low protective characteristics, in which corrosion of the substrate occurs at the base of the layer pores [39]. The scale formed at the same temperature but during a longer period (30 days) presents a diffusive behavior, which is justified on the equivalent circuit fitting (Table 7) by CPE<sub>inner</sub> with  $n = 0.5$  (Warburg impedance response). The first arc at high frequency range can be attributed to charge transfer, associated with the effect of electric double layer capacitance of the corrosive medium/corrosion products surface interface. The linear tail at low frequency range may indicate a finite thickness layer diffusion process related mainly with the fact that more compact scale was formed in CO<sub>2</sub> environment, showing a shielding effect on mass transport of reactants and products. The Nyquist plots of scales formed at 90 °C (Fig. 10(a)) show a single semicircle for both periods of growth (7 and 30 days). This impedance behavior for scales growth at higher temperature (90 °C) is related to formation of scales more compact and denser than at 50 °C

**Table 6**

Impedance modulus  $|Z|$  at low frequency (0.1 Hz) and degradation coefficient for scales formed in CO<sub>2</sub> saturated brine in function of immersion time in 0.1 M Na<sub>2</sub>SO<sub>4</sub> solution.

Scale growth conditions	$ Z $ ( $\Omega \cdot \text{cm}^2$ )			Degradation coefficient	
	1 h	24 h	168 h	24 h	168 h
50 °C, 7 days	8 ( $\pm$ 0.5) $\times 10^3$	7 ( $\pm$ 0.2) $\times 10^3$	7 ( $\pm$ 0.2) $\times 10^3$	0.05 ( $\pm$ 0.08)	0.03 ( $\pm$ 0.05)
50 °C, 30 days	9 ( $\pm$ 0.4) $\times 10^4$	5 ( $\pm$ 0.2) $\times 10^4$	1 ( $\pm$ 0.3) $\times 10^4$	0.3 ( $\pm$ 0.05)	0.8 ( $\pm$ 0.2)
90 °C, 7 days	4 ( $\pm$ 0.3) $\times 10^4$	2 ( $\pm$ 0.2) $\times 10^4$	2 ( $\pm$ 0.3) $\times 10^4$	0.2 ( $\pm$ 0.08)	0.2 ( $\pm$ 0.2)
90 °C, 30 days	3 ( $\pm$ 0.3) $\times 10^4$	8 ( $\pm$ 0.9) $\times 10^3$	4 ( $\pm$ 0.5) $\times 10^3$	0.5 ( $\pm$ 0.06)	0.9 ( $\pm$ 0.1)

due to the high rate of FeCO<sub>3</sub> nucleation and growth, as can be seen in the FE-SEM images (Fig. 5). However, the radius of the capacitive semicircle decreases in scale formed at 90 °C/30 days when compared to 90 °C/7 days, which can be related that the protective character of the scale degrades with the increase of the immersion time. The decrease of capacitive semicircle may be an indicator of electrolyte migration through the porous of scale. In the low frequency region, the phase angle (Fig. 11(c) and (d)) of the scales grown at 90 °C initially increases and then gradually decreases. This aspect also indicates that the corrosion resistance initially increases and then weakens probably related to the migration of corrosive medium through the porous in scale. In accordance with the results of the polarization curves, the EIS confirmed a higher impedance of scales formed at 90 °C than of those formed at 50 °C. Although in this present investigation the number of the times constant was not determined, the number of times constant could be determined from EIS plot shown in Fig. 10, as previously reported [37, 53]. Based on this, it is speculated that both planar and porous electrode behavior are dominating the resulting electrochemical behavior of the examined samples. Also, their corresponding domains (predominantly planar or porous) are modifying with both temperature and time of immersion carried out. However, another systematic investigation should be provided in order to elucidate and clarify these modification electrochemical domains.

The evolution of the impedance results over time (1 h, 24 h, 168 h) was also investigated for distinct scales to calculate the corresponding scales degradation coefficients. The electrochemical properties of steel covered with scales grown at 50 °C and 90 °C for 7 and 30 days, in function of immersion time in Na<sub>2</sub>SO<sub>4</sub>, are presented by Bode diagrams in Fig. 11. The evolution of the impedance modulus  $|Z|$  at low frequencies and degradation coefficients of scales over time are shown in Table 6. The scales impedance values ranged from  $8 \times 10^3$  to  $9 \times 10^4 \Omega \cdot \text{cm}^2$  after 1 h of immersion and decreased with the immersion time in Na<sub>2</sub>SO<sub>4</sub>, which means that scales can reduce protective capability.

**Table 7**

Electrochemical parameters obtained from equivalent circuit fitting of scales formed on the steel surface in CO<sub>2</sub> saturated brine in 0.1 M Na<sub>2</sub>SO<sub>4</sub>.

Scale growth conditions		50 °C, 7 days	50 °C, 30 days	90 °C, 7 days	90 °C, 30 days
CPE <sub>outer</sub>	Y <sub>o</sub> ( $\times 10^{-7} \text{ F} \cdot \text{cm}^{-2} \cdot \text{s}^{n-1}$ )	8.06 ( $\pm$ 0.64)	10.9 ( $\pm$ 0.2)	244 ( $\pm$ 0.22)	3100 ( $\pm$ 0.02)
	n	0.689 ( $\pm$ 0.009)	0.630 ( $\pm$ 0.02)	0.568 ( $\pm$ 0.10)	0.520 ( $\pm$ 0.01)
R <sub>pore/outer</sub>	( $\Omega \cdot \text{cm}^2$ )	718 ( $\pm$ 11)	650 ( $\pm$ 29)	11,326 ( $\pm$ 89)	1360 ( $\pm$ 110)
CPE <sub>inner</sub>	Y <sub>o</sub> ( $\times 10^{-5} \text{ F} \cdot \text{cm}^{-2} \cdot \text{s}^{n-1}$ )	8.17 ( $\pm$ 0.25)	7.67 ( $\pm$ 0.22)	0.86 ( $\pm$ 0.24)	15.1 ( $\pm$ 0.23)
	n	0.617 ( $\pm$ 0.007)	0.580 ( $\pm$ 0.007)	0.820 ( $\pm$ 0.04)	0.760 ( $\pm$ 0.03)
R <sub>pore/inner</sub>	( $\Omega \cdot \text{cm}^2$ )	2056 ( $\pm$ 57)	2810 ( $\pm$ 59)	61,452 ( $\pm$ 74)	12,626 ( $\pm$ 266)
CPE <sub>dl</sub>	Y <sub>o</sub> ( $\times 10^{-4} \text{ F} \cdot \text{cm}^{-2} \cdot \text{s}^{n-1}$ )	7.40 ( $\pm$ 0.24)	0.677 ( $\pm$ 0.05)	0.437 ( $\pm$ 0.003)	5.09 ( $\pm$ 0.013)
	n	0.570 ( $\pm$ 0.01)	0.760 ( $\pm$ 0.01)	0.678 ( $\pm$ 0.001)	0.930 ( $\pm$ 0.02)
R <sub>ct</sub>	( $\Omega \cdot \text{cm}^2$ )	3563 ( $\pm$ 94)	2161 ( $\pm$ 75)	35,205 ( $\pm$ 740)	10,479 ( $\pm$ 1343)
$\chi^2$		$3.5 \times 10^{-5}$	$1.12 \times 10^{-4}$	$3.30 \times 10^{-4}$	$1.05 \times 10^{-4}$

$\chi^2$  = chi-squared

Scales grown for longer periods showed higher degradation coefficients. Considering longer immersion times in electrolyte (168 h), the scale grown at 90 °C and 7 days showed the best quality of scale. The scale that presented a higher degradation coefficient was the one grown at 90 °C for 30 days. Despite the scales showed degradation with time, they provide certain protection against steel corrosion. The level of protection will depend on the environmental conditions the scales were growth. FeCO<sub>3</sub> scale covering steel surface after exposed to CO<sub>2</sub> corrosion environment in anaerobic condition was promptly examined by X-ray photoelectron spectroscopy (XPS) technique by Heuer and Stubbins [54]. They observed decomposition product (Fe<sub>2</sub>O<sub>3</sub>) which was associated to FeCO<sub>3</sub> chemical instability in air Table 7.

The use of electrical equivalent circuits is a classical approach to elucidate EIS data. Since an equivalent circuit is used in order to determine the simulated values and compare with experimental data, a CNLS (complex non-linear least squares) simulation is used, as previously reported [37,53,55,56]. The analysis of parameters from equivalent circuit fitting can provide information about resistance and capacitance of coating material, charge transfer resistance and double-layer capacitance. Several equivalent circuits were tested, with the aim of getting the best fitting to the experimental results but also of finding a circuit with a physical meaning that better represents the double layer scale. The electrical equivalent circuit chosen was proposed by Tribollet and Orazem [57] providing good fitting. The same equivalent circuit was used by Wei et al. [34] and Gao et al. [58] for FeCO<sub>3</sub> scales with duplex layer structure. This equivalent electrical circuit of

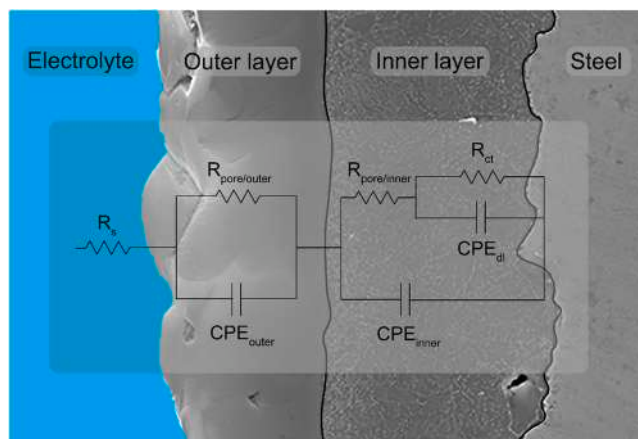


**Fig. 12.** Electrical equivalent circuit of the impedance for substrate coated by two superimposed porous layers. CPE<sub>outer</sub>: outer layer capacitance; CPE<sub>inner</sub>: inner layer capacitance; CPE<sub>dl</sub>: double layer capacitance; R<sub>pore/outer</sub>: pores outer layer resistance; R<sub>pore/inner</sub>: pores inner layer resistance; R<sub>ct</sub>: charge transfer resistance.

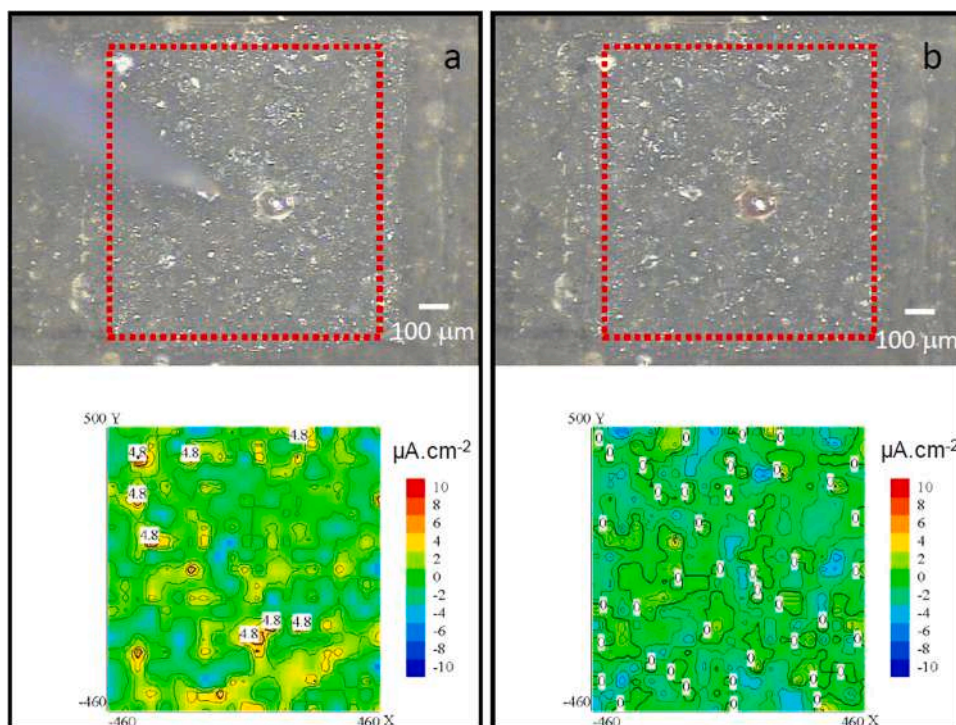


**Fig. 13.** Sample surface activity images and current density distributions for scale formed in  $\text{CO}_2$  saturated brine at  $90^\circ\text{C}$  and 30 days. (a) After 15 min of immersion in 0.1 M  $\text{Na}_2\text{SO}_4$  solution. (b) After 24 h of immersion in 0.1 M  $\text{Na}_2\text{SO}_4$  solution. X and Y correspond to dimensions of the scan in  $\mu\text{m}$ .

the impedance consider an electrode coated by two superimposed porous layers. The electrochemical system represented by the electrical circuit of Fig. 12 is characterized by a double layer capacitance ( $\text{CPE}_{\text{dl}}$ ) and a faradaic process denoted by the charge transfer resistance ( $R_{\text{ct}}$ ), connected in series with the additional resistance of the solution inside the pores ( $R_{\text{pore}}$ ). The two capacitors related to the inner and outer layers are represented by constant phase elements ( $\text{CPE}_{\text{inner}}$  and  $\text{CPE}_{\text{outer}}$ ), since the heterogeneity and porosity of the surface does not allow adjustment to an ideal capacitive response.

The electrochemical parameters obtained from equivalent circuit fitting for all scales are shown in Table 7. The scale formed at  $90^\circ\text{C}$  for 7 and 30 days presented both layers with higher resistances ( $R_{\text{pore/outer}}$ ,  $R_{\text{pore/inner}}$ ). The charge transfer was inhibited at the interface between metal and electrolyte due to the presence of scale. The charge transfer resistance ( $R_{\text{ct}}$ ) values of the steel covered with scales formed at  $90^\circ\text{C}$  are larger than those grown at  $50^\circ\text{C}$ , which suggests the formation of the protective scale (insulating properties) on the steel surface in the corrosive environment at higher temperatures. Scales that act as a good barrier maintain highly capacitive behavior. Nonetheless, an increase of resistive behavior is representative of scale degradation and active corrosion of steel substrate. The temperature has a significant influence on the protectiveness of scale once the precipitation rate of  $\text{FeCO}_3$  is faster at high temperatures and it tends to form dense scales providing good protection to the steel surface. Results of EIS are in good agreement with the study of Wu et al. [32].

Although in this present investigation the number of the time constants has been not determined, it could be obtained from EIS plots (Fig. 10) as previously reported [37,53]. Based on this, it is speculated that both planar and porous electrode behavior are dominating the resulting electrochemical compartment of the examined samples. Also, their corresponding domains (predominantly planar or porous) are modifying with both temperature and time of immersion. However, future systematic investigation can be carried out to elucidate and clarify these changes in the electrochemical domains.

When the carbon steel is exposed to the  $\text{CO}_2$  corrosion environments, the ferrite phase dissolves preferentially releasing  $\text{Fe}^{2+}$  to further form

$\text{FeCO}_3$ . If the  $\text{FeCO}_3$  scales are able to reduce the active surface areas and limit the ion mass transfer, as shown by EIS results in 0.1 M  $\text{Na}_2\text{SO}_4$  electrolyte, it is estimated that in  $\text{CO}_2$  media at high pressure the scales formed naturally on the metal surface can protect the substrate against further metal dissolution. These results agree with a decreasing on the  $\text{CO}_2$  corrosion rate over time and with increasing of temperature determined by mass loss tests (Fig. 3). Due to difficulty to perform in-situ high pressure and high temperature electrochemical tests, the study of electrochemical properties of  $\text{FeCO}_3$  scales and its degradation over time in  $\text{NaSO}_4$  solution, at standard temperature and pressure, can be an alternative to predict the scales anti-corrosion capability in  $\text{CO}_2$  environment. The main advantage of using  $\text{NaSO}_4$  solution is its strong ionic character, allowing a better assessment of the charge transference process through scale, in addition to avoid localized corrosion caused, for example, by the presence of chloride.

SVET was used to monitor the evolution of corrosion process in 0.05 M  $\text{NaCl}$  solution of scale-covered steel formed under  $90^\circ\text{C}$  for 30 days. Fig. 13 presents SVET results of the sample images and respective local current maps. Anodic currents appear in warm tones (the red color represents the highest currents) and cathodic currents appear in cold tones (dark blue represents the highest values). Currents close to zero appear in green. No detectable corrosion activity was observed on the scaled steel surface during the entire immersion time (24 h). The anodic and cathodic current densities remained at the level of noise, which is a good indication of protective behavior of the scale formed and no galvanic couple formation between scale/steel substrate was observed. There was a darkening observed near the area of the artificial defect at the end of immersion, but still no corrosion activity was detected by SVET. This suggests that, although some corrosion process could be occurring at the interface formed between steel and the inner layer of scales, the intensity of the process was very small, not enough to become detectable by the SVET probe positioned  $100\ \mu\text{m}$  above the sample surface.

## 4. Conclusions

The corrosion product scales formed on the steel surface under CO<sub>2</sub> environment are frequently considered as a naturally occurring anti-corrosion barrier. To clarify the effects of temperature and corrosion time on the protectiveness of corrosion product scales, the formation of corrosion product scales was induced on the L80 steel substrates under high pressure and high temperature CO<sub>2</sub> environments. The general CO<sub>2</sub> corrosion rate was determined, and the morphology, microstructure and chemical composition of scales were characterized. Furthermore, the properties of scales as anti-corrosion barrier were determined PD and EIS electrochemical techniques in aerated NaSO<sub>4</sub> electrolyte, and the SVET technique was used in NaCl solution to verify the occurrence or not of galvanic couple formation between scale and steel in presence of coating damage. From the research reported in this paper the following conclusions can be drawn:

1. Mass loss tests conducted on specimens of L80 API 5CT steel corroded at 50 °C and 90 °C in brine saturated with CO<sub>2</sub> at 15 MPa showed that general corrosion rates are highest at lower temperature.
2. The corrosion scales formed on the steel surface are composed of two layers, the first inner layer consisting of carbonate and cementite, due to preferential dissolution of the ferrite, and the second layer consisting only of carbonates. The formed carbonate was iron carbonate, with a small fraction of calcium as a substitutional element. The morphology and size of carbonate crystals varied according to temperature and time of exposure to the corrosive media. The thickness of corrosion scales is not directly related to the corrosion rate. However, the FE-SEM images showed that scales have different porosity and compactness characteristics, depending on the environmental conditions in which they were grown.
3. The scales formed under CO<sub>2</sub> environment can provide considerable steel protection, acting as a barrier to the diffusion of ionic species, as shown in PD curves and EIS measurements. It was observed that scales formed at 90 °C are more protective than those formed at 50 °C, and that this protection depends on time of exposure to the corrosive environment. Protective anti-corrosion capability of the scales was additionally confirmed by localized study using SVET, indicating no galvanic pair formation with steel substrate.
4. The results obtained by electrochemical tests of potentiodynamic polarization and electrochemical impedance showed that the study of the electrochemical properties of double layer and porous scales is relatively complex. The EIS is an appropriate technique to evaluate the level of steel protection provided by the scales when associated with other techniques. The proposed equivalent circuit is in good concordance with observations from the FE-SEM images and mass loss test.

## Declaration of Competing Interest

The authors declare that they have no known competing financial interests or personal relationships that could have appeared to influence the work reported in this paper.

## Data Availability

Data will be made available on request.

## Acknowledgements

The authors acknowledge the support provided by CNPq (The Brazilian Research Council) and IPR (Institute of Petroleum and Natural Resources). This study was financed in part by the Coordination for the Improvement of Higher Education Personnel – Brazil (CAPES) – Finance Code 001.

J.S. Fernandes and M. Taryba from Centro de Química Estrutural acknowledge the financial support of Fundação para a Ciência e Tecnologia (UIDB/00100/2020 and UIDP/00100/2020).

## References

- [1] R. Barker, D. Burkle, T. Charpentier, H. Thompson, A. Neville, A review of iron carbonate (FeCO<sub>3</sub>) formation in the oil and gas industry, *Corros. Sci.* 142 (2018) 312–341, <https://doi.org/10.1016/j.corsci.2018.07.021>.
- [2] M. Askari, M. Aliofkhaezaei, R. Jafari, P. Hamghalam, A. Hajizadeh, Downhole corrosion inhibitors for oil and gas production – a review, *Appl. Surf. Sci. Adv.* 6 (2021), <https://doi.org/10.1016/j.apsadv.2021.100128>.
- [3] L.T. Popoola, A.S. Grema, G.K. Latinwo, B. Gutti, A.S. Balogun, Corrosion problems during oil and gas production and its mitigation, *Int. J. Ind. Chem.* (2013) 4–35, <https://doi.org/10.1186/2228-5547-4-35>.
- [4] V. Arora, R.K. Saran, R. Kumar, S. Yadav, Separation and sequestration of CO<sub>2</sub> in geological formations, *Mater. Sci. Energy Technol.* 2 (2019) 647–656, <https://doi.org/10.1016/j.mset.2019.08.006>.
- [5] F. Gozalpour, S.R. Ren, B. Tohidi, CO<sub>2</sub> EOR and Storage in Oil Reservoirs, 2005. (<http://www.ieagreen.org.uk/sept32.htm>).
- [6] Z.D. Cui, S.L. Wu, S.L. Zhu, X.J. Yang, Study on corrosion properties of pipelines in simulated produced water saturated with supercritical CO<sub>2</sub>, *Appl. Surf. Sci.* 252 (2006) 2368–2374, <https://doi.org/10.1016/j.apsusc.2005.04.008>.
- [7] R.L.C. Beltrao, C.L. Sombra, A.C.V.M. Lage, J.R.F. Netto, C.C.D. Henriques, SS: Pre-salt Santos basin - challenges and New Technologies for the Development of the Pre-salt Cluster, Santos Basin, Brazil, *Soc. Pet. Eng. (SPE)* (2009), <https://doi.org/10.4043/19880-ms>.
- [8] A. Oliveira da Costa, F. Farias de Souza, M. Lima, F. Corrêa Ferreira, G. de Figueiredo da Costa, G. Theulen Antoniasse, R. Dias Teixeira, R. Fagundes Leggieri, R. Freitas Fernandes, V. Manuel do Espírito Santo Silva, Brazilian Oil & Gas Report 2018/2019 Trends and Recent Developments, 2019.
- [9] Y.S. Choi, D. Young, S. Nesić, L.G.S. Gray, Wellbore integrity and corrosion of carbon steel in CO<sub>2</sub> geologic storage environments: a literature review, *Int. J. Greenh. Gas. Control* 16 (2013), <https://doi.org/10.1016/j.ijggc.2012.12.028>.
- [10] C.I. Ossai, B. Boswell, L.J. Davies, Pipeline Fail. *Corros. Environ. – A Concept. Anal. Trends Eff. Am. Soc. Mech. Eng.* 53 (2015) 36–58, <https://doi.org/10.1016/j.engfailanal.2015.03.004>.
- [11] D.A. Lopez, T. Perez, S.N. Simison, The influence of microstructure and chemical composition of carbon and low alloy steels in CO<sub>2</sub> corrosion. A state-of-the-art appraisal, *Mater. Des.* 24 (2003) 561–575, <https://doi.org/10.1016/S0261-3069Z03.00158-4>.
- [12] S. Nesić, Key issues related to modelling of internal corrosion of oil and gas pipelines - a review, *Corros. Sci.* 49 (2007) 4308–4338, <https://doi.org/10.1016/j.corsci.2007.06.006>.
- [13] S. Hassani, T.N. Vu, N.R. Rosli, S.N. Esmaeely, Y.S. Choi, D. Young, S. Nesić, Wellbore integrity and corrosion of low alloy and stainless steels in high pressure CO<sub>2</sub> geologic storage environments: an experimental study, *Int. J. Greenh. Gas. Control* 23 (2014) 30–43, <https://doi.org/10.1016/j.ijggc.2014.01.016>.
- [14] P. Kritzer, Corrosion in high-temperature and supercritical water and aqueous solutions: a review, *J. Supercrit. Fluids* 29 (2004) 1–29, [https://doi.org/10.1016/S0896-8446\(03\)00031-7](https://doi.org/10.1016/S0896-8446(03)00031-7).
- [15] Y. Hua, R. Barker, A. Neville, Comparison of corrosion behaviour for X-65 carbon steel in supercritical CO<sub>2</sub>-saturated water and water-saturated/unsaturated supercritical CO<sub>2</sub>, *J. Supercrit. Fluids* 97 (2015) 224–237, <https://doi.org/10.1016/j.supflu.2014.12.005>.
- [16] A.S. Ruhl, A. Kranzmann, Corrosion in supercritical CO<sub>2</sub> by diffusion of flue gas acids and water, *J. Supercrit. Fluids* 68 (2012) 81–86, <https://doi.org/10.1016/j.supflu.2012.04.015>.
- [17] J. Zhang, Z.L. Wang, Z.M. Wang, X. Han, Chemical analysis of the initial corrosion layer on pipeline steels in simulated CO<sub>2</sub>-enhanced oil recovery brines, *Corros. Sci.* 65 (2012) 397–404, <https://doi.org/10.1016/j.corsci.2012.08.045>.
- [18] Y. Zhang, X. Pang, S. Qu, X. Li, K. Gao, Discussion of the CO<sub>2</sub> corrosion mechanism between low partial pressure and supercritical condition, *Corros. Sci.* 59 (2012) 186–197, <https://doi.org/10.1016/j.corsci.2012.03.006>.
- [19] R.A. de Motte, R. Barker, D. Burkle, S.M. Vargas, A. Neville, The early stages of FeCO<sub>3</sub> scale formation kinetics in CO<sub>2</sub> corrosion, *Mater. Chem. Phys.* 216 (2018) 102–111, <https://doi.org/10.1016/j.matchemphys.2018.04.077>.
- [20] Y.A. Meyer, R.S. Bonatti, A.D. Bortolozzo, W.R. Osório, Electrochemical behavior and compressive strength of Al-Cu/xCu composites in NaCl solution, *J. Solid State Electrochem.* 25 (2021) 1303–1317, <https://doi.org/10.1007/s10008-020-04890-x>.
- [21] L.M. Satizabal, D. Costa, P.B. Moraes, A.D. Bortolozzo, W.R. Osório, Microstructural array and solute content affecting electrochemical behavior of Sn Ag and Sn Bi alloys compared with a traditional Sn Pb alloy, *Mater. Chem. Phys.* 223 (2019) 410–425, <https://doi.org/10.1016/j.matchemphys.2018.11.003>.
- [22] Y. Guo, C. Li, Y. Liu, L. Yu, Z. Ma, C. Liu, H. Li, Effect of microstructure variation on the corrosion behavior of high-strength low-alloy steel in 3.5wt% NaCl solution, *Int. J. Miner., Metall., Mater.* 22 (2015) 604–612, <https://doi.org/10.1007/s12613-015-1113-z>.
- [23] S. Bordbar, M. Alizadeh, S.H. Hashemi, Effects of microstructure alteration on corrosion behavior of welded joint in API X70 pipeline steel, *Mater. Des.* 45 (2013) 597–604, <https://doi.org/10.1016/j.matdes.2012.09.051>.
- [24] K.K. Gupta, R. Yazdi, M. Styrk-Geisler, O.V. Mishin, R. Ambat, Effect of microstructure of low-alloy steel on corrosion propagation in a simulated CO<sub>2</sub>

- environment, *J. Electrochem Soc.* 169 (2022), 111504, <https://doi.org/10.1149/1945-7111/aca127>.
- [25] A. Pfennig, A. Kranzmann, Effects of saline aquifere water on the corrosion behaviour of injection pipe steels 1.4034 and 1.7225 during exposure to CO<sub>2</sub> environment, *Energy Procedia* (2009) 3023–3029, <https://doi.org/10.1016/j.egypro.2009.02.080>.
- [26] A. Pfennig, B. Linke, A. Kranzmann, Corrosion behaviour of pipe steels exposed for 2 years to CO<sub>2</sub>-saturated saline aquifer environment similar to the CCS-site Ketzin, Germany, in: *Energy Procedia*, Elsevier Ltd, 2011, pp. 5122–5129, <https://doi.org/10.1016/j.egypro.2011.02.488>.
- [27] M. Javidi, R. Chamanfar, S. Bekhrad, Investigation on the efficiency of corrosion inhibitor in CO<sub>2</sub> corrosion of carbon steel in the presence of iron carbonate scale, *J. Nat. Gas. Sci. Eng.* 61 (2019) 197–205, <https://doi.org/10.1016/j.jngse.2018.11.017>.
- [28] Y. Liu, H. Jiang, T. Xu, Y. Li, CO<sub>2</sub> corrosion prediction on 20# steel under the influence of corrosion product film, *Petroleum* (2021), <https://doi.org/10.1016/j.petlm.2021.07.003>.
- [29] T. Li, Y. Yang, K. Gao, M. Lu, Mechanism of protective film formation during CO<sub>2</sub> corrosion of X65 pipeline steel, *J. Univ. Sci. Technol. Beijing: Miner. Metall. Mater. (Eng. Ed.)* 15 (2008) 702–706, [https://doi.org/10.1016/S1005-8850\(08\)60274-1](https://doi.org/10.1016/S1005-8850(08)60274-1).
- [30] X. Li, Y. Zhao, W. Qi, J. Xie, J. Wang, B. Liu, G. Zeng, T. Zhang, F. Wang, Effect of extremely aggressive environment on the nature of corrosion scales of HP-13Cr stainless steel, *Appl. Surf. Sci.* 469 (2019) 146–161, <https://doi.org/10.1016/j.apsusc.2018.10.237>.
- [31] Y. Xiang, Z. Wang, M. Xu, Z. Li, W. Ni, A mechanistic model for pipeline steel corrosion in supercritical CO<sub>2</sub>-SO<sub>2</sub>-O<sub>2</sub>-H<sub>2</sub>O environments, *J. Supercrit. Fluids* 82 (2013) 1–12, <https://doi.org/10.1016/j.supflu.2013.05.016>.
- [32] S.L. Wu, Z.D. Cui, G.X. Zhao, M.L. Yan, S.L. Zhu, X.J. Yang, EIS study of the surface film on the surface of carbon steel from supercritical carbon dioxide corrosion, *Appl. Surf. Sci.* 228 (2004) 17–25, <https://doi.org/10.1016/j.apsusc.2003.12.025>.
- [33] American Petroleum Institute. Specification for Casing and Tubing. API Specification 5CT 9th ed. Washington: American Petroleum Institute; 2011.
- [34] D. Li, Z. Duan, The speciation equilibrium coupling with phase equilibrium in the H<sub>2</sub>O-CO<sub>2</sub>-NaCl system from 0 to 250 °C, from 0 to 1000 bar, and from 0 to 5 molality of NaCl, *Chem. Geol.* 244 (2007) 730–751, <https://doi.org/10.1016/j.chemgeo.2007.07.023>.
- [35] ASTM International G1–03, Standard Practice for Preparing, Cleaning, and Evaluation Corrosion Test Specimens, 2003.
- [36] S. Arzola, M.E. Palomar-Pardavé, J. Genesca, Effect of resistivity on the corrosion mechanism of mild steel in sodium sulfate solutions, *J. Appl. Electrochem* 33 (2003) 1223–1231.
- [37] T. Duarte, Y.A. Meyer, W.R. Osório, The Holes of Zn phosphate and hot dip galvanizing on electrochemical behaviors of multi-coatings on steel substrates, *Metals* 12 (2022) 863, <https://doi.org/10.3390/met12050863>.
- [38] X.L. Zhang, Zh.H. Jiang, Zh.P. Yao, Y. Song, Zh.D. Wu, Effects of scan rate on the potentiodynamic polarization curve obtained to determine the Tafel slopes and corrosion current density, *Corros. Sci.* 51 (2009) 581–587, <https://doi.org/10.1016/j.corsci.2008.12.005>.
- [39] E. McCafferty, Validation of corrosion rates measured by the Tafel extrapolation method, *Corros. Sci.* 47 (2005) 3202–3215, <https://doi.org/10.1016/j.corsci.2005.05.046>.
- [40] X. Yue, L. Zhang, Y. Hua, Fundamental insights into the stabilisation and chemical degradation of the corrosion product scales, *Npj Mater. Degrad.* 5 (2021), <https://doi.org/10.1038/s41529-021-00152-x>.
- [41] J.L. Crolet, N. Thevenot, S. Nestic, Role of conductive corrosion products on the protectiveness of corrosion layers, *NACE - Int. Corros. Conf. Ser.* 1996-March (1996) 194–203.
- [42] G. Cui, Z. Yang, J. Liu, Z. Li, A comprehensive review of metal corrosion in a supercritical CO<sub>2</sub> environment, *Int. J. Greenh. Gas. Control* 90 (2019), <https://doi.org/10.1016/j.ijggc.2019.102814>.
- [43] L. Wei, X. Pang, C. Liu, K. Gao, Formation mechanism and protective property of corrosion product scale on X70 steel under supercritical CO<sub>2</sub> environment, *Corros. Sci.* 100 (2015) 404–420, <https://doi.org/10.1016/j.corsci.2015.08.016>.
- [44] T. Berntsen, M. Seiersten, T. Hemmingsen, Effect of FeCO<sub>3</sub> supersaturation and carbide exposure on the CO<sub>2</sub> corrosion rate of carbon steel, *Corrosion* 69 (2013) 601–613.
- [45] Y. Hua, S. Xu, Y. Wang, W. Taleb, J. Sun, L. Zhang, R. Barker, A. Neville, The formation of FeCO<sub>3</sub> and Fe<sub>3</sub>O<sub>4</sub> on carbon steel and their protective capabilities against CO<sub>2</sub> corrosion at elevated temperature and pressure, *Corros. Sci.* 157 (2019) 392–405, <https://doi.org/10.1016/j.corsci.2019.06.016>.
- [46] L.M. Tavares, E.M. da Costa, J.J.D.O. Andrade, R. Hubler, B. Huet, Effect of calcium carbonate on low carbon steel corrosion behavior in saline CO<sub>2</sub> high pressure environments, *Appl. Surf. Sci.* 359 (2015) 143–152, <https://doi.org/10.1016/j.apsusc.2015.10.075>.
- [47] R. Rizzo, S. Gupta, M. Rogowska, R. Ambat, Corrosion of carbon steel under CO<sub>2</sub> conditions: effect of CaCO<sub>3</sub> precipitation on the stability of the FeCO<sub>3</sub> protective layer, *Corros. Sci.* 162 (2020), <https://doi.org/10.1016/j.corsci.2019.108214>.
- [48] F. Farelas, M. Galicia, B. Brown, S. Nestic, H. Castaneda, Evolution of dissolution processes at the interface of carbon steel corroding in a CO<sub>2</sub> environment studied by EIS, *Corros. Sci.* 52 (2010) 509–517, <https://doi.org/10.1016/j.corsci.2009.10.007>.
- [49] A. Shatskiy, Y.M. Borzdov, K.D. Litasov, I.N. Kupriyanov, E. Ohtani, Y.N. Palyanov, Phase relations in the system FeCO<sub>3</sub>-CaCO<sub>3</sub> at 6 GPa and 900–1700 °C and its relation to the system CaCO<sub>3</sub>-FeCO<sub>3</sub>-MgCO<sub>3</sub>, *Am. Mineral.* 99 (2014) 773–785, <https://doi.org/10.2138/am.2014.4721>.
- [50] L. Donald, Graf, *Crystallographic tables for the rhombohedral carbonates*, *Am. Mineral.* 46 (1961) 1283–1316.
- [51] A. Kahyarian, B. Brown, S. Nestic, Electrochemistry of CO<sub>2</sub> corrosion of mild steel: Effect of CO<sub>2</sub> on iron dissolution reaction, *Corros. Sci.* 129 (2017) 146–151, <https://doi.org/10.1016/j.corsci.2017.10.005>.
- [52] C. Wang, Y. Hua, S. Nadimi, W. Taleb, R. Barker, Y. Li, X. Chen, A. Neville, Determination of thickness and air-void distribution within the iron carbonate layers using X-ray computed tomography, *Corros. Sci.* 179 (2021), <https://doi.org/10.1016/j.corsci.2020.109153>.
- [53] B. Hirschorn, M.E. Orazem, B. Tribollet, V. Vivier, I. Frateur, M. Musiani, Determination of effective capacitance and film thickness from constant-phase-element parameters, *Electro Acta* 55 (2010) 6218–6227, <https://doi.org/10.1016/j.jelectacta.2009.10.065>.
- [54] J.K. Heuer, J.F. Stubbins, An XPS characterization of FeCO<sub>3</sub> from CO<sub>2</sub> corrosion, *Corros. Sci.* 41 (1999) 1231–1243.
- [55] B. Hirschorn, M.E. Orazem, B. Tribollet, V. Vivier, I. Frateur, M. Musiani, Constant-phase-element behavior caused by resistivity distributions in films, *J. Electrochem Soc.* 157 (2010) C458, <https://doi.org/10.1149/1.3499565>.
- [56] Y.A. Meyer, I. Menezes, R.S. Bonatti, A.D. Bortolozzo, W.R. Osório, EIS investigation of the corrosion behavior of steel bars embedded into modified concretes with eggshell contents, *Metals* 12 (2022) 417, <https://doi.org/10.3390/met12030417>.
- [57] M.E. Orazem, B. Tribollet, *Electrochemical Impedance Spectroscopy*, John Wiley & Sons, Inc, Hoboken, NJ, USA, 2008, <https://doi.org/10.1002/9780470381588>.
- [58] M. Gao, X. Pang, K. Gao, The growth mechanism of CO<sub>2</sub> corrosion product films, *Corros. Sci.* 53 (2011) 557–568, <https://doi.org/10.1016/j.corsci.2010.09.060>.